

Adaptive Non-local Observable on Quantum Neural Networks

Hsin-Yi Lin^{1*}, Huan-Hsin Tseng^{2†}, Samuel Yen-Chi Chen^{3‡}, Shinjae Yoo^{2§}

¹Department of Mathematics and Computer Science, Seton Hall University, South Orange, NJ, USA

²AI & ML Department, Brookhaven National Laboratory, Upton, NY, USA

³Wells Fargo, New York, NY, USA

Email: * hsinyi.lin@shu.edu, † htseng@bnl.gov, ‡ yen-chi.chen@wellsfargo.com, § syjoo@bnl.gov

Abstract—Conventional Variational Quantum Circuits (VQCs) for Quantum Machine Learning typically rely on a fixed Hermitian observable, often built from Pauli operators. Inspired by the Heisenberg picture, we propose an *adaptive non-local measurement* framework that substantially increases the model complexity of the quantum circuits. Our introduction of *dynamical Hermitian observables* with evolving parameters shows that optimizing VQC rotations corresponds to tracing a trajectory in the observable space. This viewpoint reveals that standard VQCs are merely a special case of the Heisenberg representation.

Furthermore, we show that properly incorporating variational rotations with non-local observables enhances qubit interaction and information mixture, admitting flexible circuit designs. Two non-local measurement schemes are introduced, and numerical simulations on classification tasks confirm that our approach outperforms conventional VQCs, yielding a more powerful and resource-efficient approach as a Quantum Neural Network.

Index Terms—Variational Quantum Circuits, Quantum Machine Learning, Quantum Neural Networks, non-local observables, Heisenberg representations, Hermitian operators, classifications.

I. INTRODUCTION

Quantum Machine Learning (QML) is a developing field that leverages the principles of quantum mechanics to advance machine learning (ML) models. With the rapid advancement of quantum computing hardware, QML aims to exploit quantum phenomena—such as superposition, entanglement, and quantum interference—to provide computational advantages over classical approaches. Despite the current limitations of quantum hardware, hybrid quantum-classical algorithms have been developed to harness the strengths of both computing paradigms, allowing near-term quantum devices to contribute meaningfully to real-world ML tasks.

One of the most promising classes of hybrid quantum-classical algorithms is Variational Quantum Algorithms (VQAs) [1]–[4]. These algorithms optimize quantum circuit parameters using classical optimization techniques, including

This work is supported by the U.S. DOE, under award DE-SC-0012704 and BNL's LDRD #24-061. This research used resources of the NERSC, under Contract No. DE-AC02-05CH11231 using NERSC award HEP-ERCAP0033786.

The views expressed in this article are those of the authors and do not represent the views of Wells Fargo. This article is for informational purposes only. Nothing contained in this article should be construed as investment advice. Wells Fargo makes no express or implied warranties and expressly disclaims all legal, tax, and accounting implications related to this article.

gradient-based methods [5], [6] and gradient-free approaches such as surrogate methods [7], simultaneous perturbation stochastic approximation (SPSA) [8], evolutionary algorithms [9], and trust region methods like COBYLA for constrained variational optimization.

VQA is a fundamental optimization framework for various quantum models. Variational Quantum Eigensolver (VQE) [10]–[12] is one such example, leveraging the VQA approach to approximate the ground state energy of a given Hamiltonian, making it particularly useful for quantum chemistry and material science. Another example is the Quantum Neural Network (QNN), which also employs the VQA framework but with the goal of fitting data for different machine learning applications. QNNs have been successfully applied to diverse ML tasks and scenarios, including classification [13]–[16], time-series prediction [17], [18], data compression [19], reinforcement learning [20], generative modeling [21] and natural language processing [22]–[25]. The explainability of the QNN classifier was also investigated in [26].

Variational Quantum Circuits (VQCs), or parameterized quantum circuits (PQCs) [27], often serve as building blocks for QNN implementation. In conventional QNN architectures, local measurements are applied, where multiple basis measurements are performed on single qubits. Specifically, VQCs utilize Pauli observables ($\sigma_x, \sigma_y, \sigma_z$) to compute expectation values $\langle \psi | \sigma_i | \psi \rangle$. These expectation values serve as outputs for classification, regression, or loss function calculations in hybrid quantum-classical models.

However, the limited connectivity of qubits in near-term quantum hardware significantly restricts the function space of VQCs, reducing model expressivity. This leads to low model capacity, hampering the ability of QNNs to effectively fit complex data distributions. While most QNN implementations rely on single-qubit measurements, certain strategies have been explored to incorporate multi-qubit measurements to improve model performance. For example, instead of measuring individual qubits separately, parity measurements determine whether the number of qubits in the $|1\rangle$ state is even or odd. This method has been applied in error detection [28] and quantum classifiers [29]. Another example is the pooling measurements in Quantum Convolutional Neural Networks (QCNNs). QCNNs are inspired by classical CNNs and employ multi-qubit pooling operations to extract hierarchical features

from quantum data [30]. These operations enhance QNNs' ability to process large-scale structured data. While these approaches improve model expressivity, they remain constrained by fixed measurement operators. Recently, a learnable observable framework [31] has been introduced, demonstrating improved performance by optimizing not only the circuit parameters but also the measurement observables. To further expand QNN capacity, non-local measurements—where observables act on multiple qubits—offer a promising alternative.

In this paper, we propose an innovative variational non-local measurement framework that significantly enhances QNN expressivity. Instead of relying on single-qubit observables, we consider trainable multi-qubit Hermitian matrices as observables. These observables are optimized jointly with standard variational quantum rotation angles, allowing the model to dynamically adapt its measurement strategy during training.

Through simulations, we demonstrate that our learnable observable framework outperforms VQCs with single-qubit observables. This improvement is attributed to the increased flexibility in measurement space, which allows the model to better capture complex correlations in data. Our experimental results further validate the superior performance of this approach, highlighting the advantages of trainable non-local observables in enhancing QNN capacity.

In sum, our **key contributions** are as follows:

- Investigate the quantum circuit prediction mechanism, revealing the relation between VQCs and the dynamical Hermitian observables.
- Introduce Adaptive Non-Local Observable (ANO) framework and investigates the non-local effect from theoretical and empirical perspectives.
- Devise two practical measurement schemes (sliding k -local and pairwise combinatorial strategies) to operate ANO and provide strong empirical performance with improved parameter efficiency on real-world classification tasks.

By enabling greater measurement flexibility, our method significantly enhances QNNs' ability to learn complex functions, paving the way for more powerful quantum machine learning models.

The rest of the paper is organized as follows. In Sec. II, we highlight relevant work in previous literature. The details of the proposed framework are described in Sec. III. The general structure of VQC is reviewed in Sec. III-A, followed by the discussion of variational non-local quantum measurements in Sec. III-C and model complexity in Sec. III-D. To validate the proposed method, the experimental setup and results are explained in Sec. IV. Finally, the conclusions are summarized in Sec. V.

II. RELATED WORK

Measurement design is central to observable estimation and model performance, yet it has often been treated as a fixed component. Several studies have investigated ways to enhance measurement efficiency. One approach is to consider locally randomized measurements [32]–[35]. These works introduce

local randomness into the measurement process, typically through random single-qubit unitaries, to extract statistical information with scalable protocols for efficient estimations of quantum systems.

Other than randomized strategies, there is also growing interest in adaptive and learnable measurement strategies as a pathway toward more efficient and accurate quantum inference. For instance, [36] utilizes fixed and overcomplete POVMs (e.g., randomized Pauli measurements) to enhance observable estimation accuracy by learning optimized dual estimators that minimize variance. A more explicit form of learnable measurement is introduced in [37], where POVMs are parameterized as linear combinations of Pauli operators and jointly optimized with the quantum circuit via gradient descent. The measurement basis in this case is actively adapted during training to reduce estimation variance. Similarly, [38] reconstructs fixed but unknown POVMs through classical post-processing and explores Bayesian adaptive measurement strategies that dynamically select measurements from a predefined set (e.g., Pauli operators) to maximize information gain.

More recently, the adaptive approach is employed for QML in [31], where general single-qubit measurements were considered. Instead of considering Pauli observables as previous works, they apply parameterized Hermitian observables, which are co-trained with the variational rotation gates. The observable itself is adaptive and learned in a differentiable manner, enhancing the model beyond what fixed Pauli measurements can offer for machine learning tasks.

Motivated by these developments, this work proposes adaptive non-local measurements for QML, aimed at substantially increasing the expressivity of QNN while maintaining resource efficiency. In contrast to prior approaches that restrict measurements to single-qubit observables or fixed local POVMs, we introduce parameterized multi-qubit observables as part of the QNN architecture. This design allows the model to capture non-local quantum correlations essential for representing twisted decision boundaries and learning complex data structures.

III. VQC WITH TRAINABLE NON-LOCAL HERMITIANS

A. General VQC Structure

Quantum computing utilizes the foundation of spinor dynamics. A qubit is a spin-1/2 particle described by a spin state (wavefunction) $|\psi\rangle = c_0|0\rangle + c_1|1\rangle$ with $c_0, c_1 \in \mathbb{C}$ such that the 1-qubit Hilbert space is $\mathcal{H}^1 \cong \mathbb{C}^2$ with the standard Hermitian metric $\langle \cdot, \cdot \rangle_{\mathbb{C}^2}$. Multi-qubits are described by multi-particle states of tensor products,

$$|\psi\rangle = \sum_{i_1, \dots, i_n} c_{i_1, \dots, i_n} |i_1\rangle \otimes \dots \otimes |i_n\rangle \quad (1)$$

for $i_1, \dots, i_n \in \{0, 1\}$ with $c_{i_1, \dots, i_n} \in \mathbb{C}$. Vectors $|i_1, \dots, i_n\rangle := |i_1\rangle \otimes \dots \otimes |i_n\rangle$ form an orthonormal basis for the n -qubit Hilbert space $\mathcal{H}^n \cong \mathbb{C}^{2^n}$. A unitary operator U (also called a quantum *gate*) then transforms from one state $|\psi\rangle \in \mathcal{H}^n$ to another preserving the norm, $\langle U\psi|U\psi\rangle_{\mathbb{C}^{2^n}} =$

$\langle \psi | \psi \rangle_{\mathbb{C}^{2^n}} = 1$. We denote the collection of all gates by $\mathcal{U}(\mathcal{H}^n) = \{U : \mathcal{H}^n \rightarrow \mathcal{H}^n \mid UU^\dagger = U^\dagger U = I_{2^n}\}$.

A VQC is an approach to realize QML by seeking proper unitary transformations in $\mathcal{U}(\mathcal{H}^n)$ to fit and learn data.

Specifically, let a classical dataset be $\mathcal{D} = \{(x^{(j)}, y^{(j)}) \mid x^{(j)} \in \mathbb{R}^n, y^{(j)} \in \mathbb{R}, j \in \mathbb{N}\}$ where $x^{(j)}$ denotes an input of sample j and $y^{(j)}$ as the corresponding label. The VQC entails three steps to fit \mathcal{D} (Fig. 1):

- 1) **Encoding:** mapping a classical data $x \in \mathbb{R}^n$ (ignoring sample index j for simplicity) to $V(x) \in \mathcal{U}(\mathcal{H}^n)$ by a choice of $V : \mathbb{R}^n \rightarrow \mathcal{U}(\mathcal{H}^n)$ and a random initial $|\psi_0\rangle \in \mathcal{H}^n$. Then

$$|\psi_x\rangle := V(x) |\psi_0\rangle \quad (2)$$

embedded with the information of x is called an *encoded* state.

- 2) **Variation:** A unitary $U(\theta) \in \mathcal{U}(\mathcal{H}^n)$ of tunable parameters θ is built to further transform $|\psi_x\rangle$ in (2). Freely adjusting parameters θ allows $U(\theta)|\psi_x\rangle$ to navigate different states in \mathcal{H}^n as much as possible.
- 3) **Measurement:** A constant Hermitian operator H is chosen such that $\langle \psi | H | \psi \rangle$ yields a real number, viewed as a VQC prediction to approach a designated target y .

Typical constructions of quantum circuits include combinations of Hadamard gate H , CNOT gate C , and gates generated by Pauli matrices $\mathcal{P} = \{I, \sigma_1, \sigma_2, \sigma_3\}$, $\phi \mapsto \{e^{-\frac{i}{2}\phi\sigma_1}, e^{-\frac{i}{2}\phi\sigma_2}, e^{-\frac{i}{2}\phi\sigma_3}\}$, also called *rotation gates* denoted by $\{R_x(\phi), R_y(\phi), R_z(\phi)\}$, respectively. For example, an n -qubit *encoding* of input $x = (x_1, \dots, x_n) \in \mathbb{R}^n$ can be,

$$V(x) = \bigotimes_{q=1}^n \left(e^{-\frac{i}{2}x_q \sigma_{k_q}} \circ H \right) \quad (3)$$

with Pauli matrix index $k_q \in \{0, 1, 2, 3\}$ of $|\mathcal{P}|$. Similarly, a multi-qubit variational gate can be constructed as follows,

$$U(\theta) = \prod_{\ell=1}^L \left(\bigotimes_{q=1}^n e^{-\frac{i}{2}\theta_q^{(\ell)} \sigma_q} \right) \circ C_\ell \in \mathcal{U}(\mathcal{H}^n) \quad (4)$$

with tunable parameters $\theta = (\theta_1^{(1)}, \dots, \theta_n^{(L)}) \in \mathbb{R}^{n \times L}$ (Fig. 1).

The three steps above together yield a VQC function,

$$\langle H \rangle(x; \theta) := \langle \psi_0 | V^\dagger(x) U^\dagger(\theta) H U(\theta) V(x) | \psi_0 \rangle \quad (5)$$

with a loss function to guide the search of parameters θ under \mathcal{D} such as,

$$L(\theta; \mathcal{D}) = \frac{1}{|\mathcal{D}|} \sum_{j=1}^{|\mathcal{D}|} \| \langle H \rangle(x^{(j)}; \theta) - y^{(j)} \|^2 \quad (6)$$

It is important to note that the variational $U(\theta)$ is the *only* learnable component in the VQC, while the encoding map V and the measurement Hermitian H remain fixed. Thus, the goal of the VQC is to find a proper $U(\theta)$ minimizing the prediction loss (6).

Hermitian measurements, also referred to as **observables**, carry important meanings in physics, such as energy distributions of quantum systems. However, the significance of their

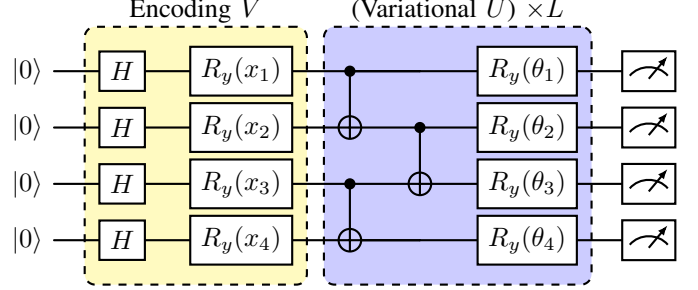


Fig. 1: A VQC diagram of (3), (4), which is also implemented in Sec. IV. The variational block represented by a blue box is repeated L times to increase the circuit depth.

roles in VQCs is seldom discussed when the standard choice is a fixed Pauli matrix in \mathcal{P} . Motivated by the Heisenberg and the Interaction pictures in Quantum Mechanics, we investigate alternative viewpoints on how these observables contribute to the VQC's prediction mechanism.

One inspiration for this proposed method is the Heisenberg representation and the interaction picture. Recall that the Heisenberg picture [39] provides a distinct view as opposed to Schrödinger's in the early development of Quantum Mechanics. Heisenberg's interpretation was that quantum evolution is characterized by *dynamical observables* (Hermitian operators), while quantum states remain static. Current VQC majorly adopts Schrödinger's perspective, where states evolve in time via unitary transformations, such as the movement in the Bloch sphere.

B. Adaptive Non-local Observables

We propose adaptive non-local observables (ANO) as a generalization to the conventional VQC by considering the following form of the **k -local observable**.

Consider an n -qubit system and $k \leq n$. Let $K = 2^k$, an adaptive k -local observable

$$H(\phi) = \begin{pmatrix} c_{11} & a_{12} + ib_{12} & a_{13} + ib_{13} & \cdots & a_{1K} + ib_{1K} \\ * & c_{22} & a_{23} + ib_{23} & \cdots & a_{2K} + ib_{2K} \\ * & * & c_{33} & \cdots & a_{3K} + ib_{3K} \\ \vdots & \vdots & \vdots & \ddots & \vdots \\ * & * & * & \cdots & c_{KK} \end{pmatrix} \quad (7)$$

where $\phi = (a_{ij}, b_{ij}, c_{ii})_{i,j=1}^K$ are arbitrary K^2 real numbers $\left(2 \times \frac{K(K-1)}{2} + K\right)$ and the lower triangle entries are defined by the corresponding complex conjugates such that $H(\phi) = (h_{ij}) = (\overline{h_{ji}}) = H^\dagger(\phi)$.

An important observation is that the variational rotation $U(\theta)$ in (5) rotates from one Hermitian H to *another*:

$$H \mapsto U^\dagger(\theta) H U(\theta). \quad (8)$$

Indeed, one sees that if we define $H(\theta) \stackrel{\text{def}}{=} U^\dagger(\theta) H U(\theta)$, it is also Hermitian whenever $U(\theta)$ is unitary. From the viewpoint of (8), it amounts to saying that the VQC is to find an *optimal observable* $H(\theta)$ minimizing loss (6), Fig. 2. Consequently,

admitting direct search for Hermitian observables *not only* includes the conventional VQC and also potentially allows one to omit the variational gate $U(\theta)$ optimization.

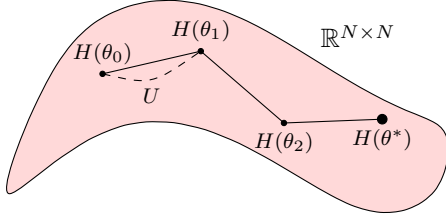


Fig. 2: By (8), a VQC varying $U(\theta)$ is equivalent to searching for observable $H(\theta) := U^\dagger(\theta) H U(\theta)$ minimizing loss (6).

It is worth noticing that the typical 1-parameter subgroup parametrization method, such as $\theta \mapsto e^{\theta A}$ of a unitary group $\mathcal{U}(\mathcal{H}^1)$, does not directly translate to $\mathbb{H}(k)$. In fact, the set of all Hermitian operators on k -qubits, denoted as $\mathbb{H}(k) = \{H : \mathcal{H}^k \rightarrow \mathcal{H}^k \mid H = H^\dagger\}$, does not form a Lie group (not even a group). Without the Lie structures (group, algebra), we opt to parameterize ANO by the formulation (7).

Note that the mapping $\phi \mapsto H(\phi)$ in (7) establishes an isomorphism from \mathbb{R}^{K^2} to $\mathbb{H}(k)$, which indicates any observable has a unique correspondence ϕ and vice versa. (7) yields ***k*-local observables** in general due to the following relation.

Definition 1 (Exact *k*-local operator). *Let $\mathcal{L}(\mathcal{H}^n)$ denotes all linear transformations on \mathcal{H}^n . If $A \in \mathcal{L}(\mathcal{H}^n)$ is called an exact *k*-local operator ($k \leq n$) if it can be written as*

$$A = I \otimes \cdots \otimes I \otimes Q \otimes I \otimes \cdots \otimes I, \quad (9)$$

where $Q \in \mathcal{L}(\mathcal{H}^k)$ acts non-trivially on **exactly *k*** of the n qubits with I denoting the identity on the remaining qubits.

Indeed, for $Q \in \mathcal{L}(\mathcal{H}^k)$ in (9), let a vector $v \in \mathcal{H}^k$ be represented by a tensorial basis $\beta = \{e_{i_1} \otimes \cdots \otimes e_{i_k}\}_{i_1, \dots, i_k}$,

$$v = \sum_{i_1, \dots, i_k}^d v_{i_1, \dots, i_k} e_{i_1} \otimes \cdots \otimes e_{i_k} \quad (10)$$

with $v_{i_1, \dots, i_k} \in \mathbb{C}$ and $\{e_1, e_2, \dots, e_d\}$ a basis of \mathcal{H}^1 . Then,

$$\begin{aligned} Qv &= \sum_{i_1, \dots, i_k} v_{i_1, \dots, i_k} Q(e_{i_1} \otimes \cdots \otimes e_{i_k}) \\ &= \sum_{i_1, \dots, i_k}^d \sum_{j_1, \dots, j_k}^d Q_{i_1, \dots, i_k}^{j_1, \dots, j_k} v_{i_1, \dots, i_k} e_{j_1} \otimes \cdots \otimes e_{j_k} \end{aligned} \quad (11)$$

where $[Q]_\beta = (Q_{i_1, \dots, i_k}^{j_1, \dots, j_k}) \in \mathbb{C}^{d^k \times d^k}$ is the matrix representation of β . Then (11) can be written in β as

$$[Qv]_\beta = [Q]_\beta [v]_\beta = \begin{pmatrix} & \vdots & \\ \cdots & Q_{i_1, \dots, i_k}^{j_1, \dots, j_k} & \cdots \\ & \vdots & \end{pmatrix} \begin{pmatrix} v_1 \\ v_2 \\ \vdots \\ v_{d^k} \end{pmatrix} \quad (12)$$

If Q is Hermitian and non-trivial, the matrix elements are written in (7). Thus, (7) represents an n -local observable in general.

To connect with the previous literature, we note that our definition of the exact k -local operator is strictly contained in the usual definition of k -local operators [40], which includes all exact r -locals of $r \leq k$. For instance, a 2-local Hamiltonian of spin glass [41],

$$H = \sum_{i, j \in E} J_{ij} \sigma_z^{(i)} \otimes \sigma_z^{(j)} + \sum_{i \in V} c_i \sigma_z^{(i)}$$

contains *exact* 2-locals of the form $\sigma_z^{(i)} \otimes \sigma_z^{(j)}$ at site (i, j) and 1-locals $\sigma_z^{(i)}$.

We also remark that the prior work [31] considered the special case of **1-local** observables,

$$H_1 \otimes I \otimes \cdots \otimes I, \quad I \otimes H_2 \otimes \cdots \otimes I, \dots, \quad I \otimes \cdots \otimes H_n, \quad (13)$$

with $H_i \in \mathcal{L}(\mathcal{H}^1)$ and have shown that learning to measure 1-local observables outperforms the conventional VQC, even as (13) are not sufficient to represent arbitrary measurements yet.

C. Navigating Observable Space via ANO

Given an n -qubit system, the parameterization (7) allows us to explore the space $\mathbb{H}(n)$. A natural question to ask is: for any two Hermitian $H_1, H_2 \in \mathbb{H}(n)$,

$$\text{Is there a } U \in \mathcal{U}(\mathcal{H}^n) \text{ such that } H_2 = U^\dagger H_1 U? \quad (14)$$

This can be viewed as an inverse operation of (8). If this is possible, the trajectories of adaptive Hermitians in ANO would be equivalent to the variational unitary operators in VQC via this 1-1 correspondence, see Fig. 3.

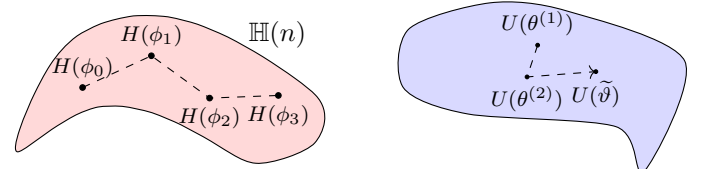


Fig. 3: [Left] Transitions in observable space $\mathbb{H}(n)$ when parametrizing from $\phi_1 \rightarrow \phi_2$ via (7). [Right] The corresponding transition in $\mathcal{U}(\mathcal{H}^n)$ via (14).

However, (14) is *not* always true. The fact that (14) does not always hold indicates our proposed ANO contains a wider function class than the conventional VQC. This claim follows from the following result,

Definition 2 (Unitary Similarity). *Let $H_1, H_2 \in \mathbb{H}(n)$. If there exists $U \in \mathcal{U}(\mathcal{H}^n)$ such that $H_1 = U^\dagger H_2 U$ then H_1 and H_2 are said to be **unitarily similar**, denoted by $H_1 \sim H_2$.*

Immediately, we recognize the unitary similarity forms an *equivalence relation* (reflexive, symmetric, and transitive). Since any Hermitian matrix is diagonalizable [42], let $H \in \mathbb{H}(n)$ and write $H = U^\dagger \Lambda U$ for some unitary U with

$\Lambda = \text{diag}(\lambda_1, \dots, \lambda_{2^n})$. As the eigenvalues of a Hermitian matrix must be *real*, then $H \sim \Lambda \cong \mathbb{R}^{2^n}$ which implies the equivalence classes $\mathbb{H}(n)/\sim$ can be represented by \mathbb{R}^{2^n} . This leads us to the following conclusion.

Theorem. *The unitary similarity defines an equivalence relation on $\mathbb{H}(n)$ and the resulting quotient space (collection of equivalence classes) $\mathbb{H}(n)/\sim$ can be identified with \mathbb{R}^{2^n} .*

This tells us that the unitary similarity partitions the observable space $\mathbb{H}(n)$ into categories of \mathbb{R}^{2^n} , see Fig. 4. Note that the theorem can be regarded as a variant of Sylvester Theorem [42].

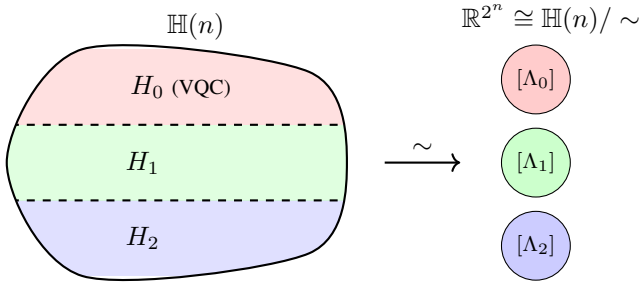


Fig. 4: Observable space $\mathbb{H}(n)$ is partitioned into equivalent classes labeled by \mathbb{R}^{2^n} . In other words, $\mathbb{H}(n)$ is classified by its eigenvalues, and VQC falls in only one particular class.

Looking back, now we see when (14) holds: it is precisely when two Hermitians share the *same eigenvalues*. Consequently, the conventional VQC is a **special case** of ANO as it operates within only one single equivalence class, Fig. 4. Indeed, the conventional VQC selects and fixes an observable H_0 to perform rotations $U(\theta)$ by (8) to minimize loss (6). By the theorem, VQC is thereby confined in the equivalence class $[H_0]$, making it a restricted case of ANO.

Furthermore, Rayleigh Quotient [42] depicts that the VQC output (5) is bounded by the eigenvalues of an observable H ,

$$\lambda_{\min} \leq \langle \psi, H\psi \rangle \leq \lambda_{\max} \quad (15)$$

with normalized state $\|\psi\| = 1$ and $\lambda_{\min} \leq \dots \leq \lambda_{\max}$ eigenvalues of H .

Therefore, VQCs with fixed Pauli observables \mathcal{P} will be further restricted in the equivalent class of $\lambda_{\min} = -1$ and $\lambda_{\max} = +1$ to limit the prediction range $-1 \leq \langle \psi, H\psi \rangle \leq 1$, making it impossible to learn targets (labels) $y > 1$ and thus leaving loss (6) irreducible. While manual normalization on data is usually a common remedy, there exist occasions where such an operation is not suitable, such as when VQC serves as a middle layer or an encoder of an Auto-Encoder.

In contrast, ANO allows H to have a broader spectrum, increases the circuit output range, and therefore improves the model capabilities. This ability to navigate different classes of equivalence (different eigenvalues) differentiates ANO from the conventional VQC in Sec. III-A.

D. *k*-local ANO with Variational Rotations

Theoretically, *full* ANO ($k = n$) guarantees the coverage of all observable classes in $\mathbb{H}(n)$ (Fig. 4). However, in practice, the number of parameters grows rapidly with the number of qubits, especially when high-dimensional features are involved. In addition to the cost, excessive parameters can increase the risk of overfitting, similar to those observed in [43]. These considerations urge us to investigate further the cases of smaller k -local ($k < n$) measurements and explore efficient ways to alleviate the limitation of smaller qubit connectivity.

Our investigation reveals that incorporating variational rotations with non-local ANO would assist *feature interactions*, which is essential for model expressivity. To demonstrate this effect of rotations on ANO, we calculate explicitly to compare the model formulation on a 2-qubit system with: (1) only 1-local ANO and (2) 1-local ANO joining variational rotations in the following example.

Example 1 (k -local ANO + rotations). We use a simple 2-qubit system (Fig. 5, 6) to show the following model capacity relations.

$$1\text{-local} \subseteq [1\text{-local} + \text{variational rotations}] \subseteq 2\text{-local}. \quad (*)$$

Assume circuits in Fig. 5, 6 have same encoding circuit V and initial $|\psi_0\rangle$. Denote the encoded state as

$$|\psi\rangle := V|\psi_0\rangle = (v_1, v_2, v_3, v_4) \in \mathbb{C}^4$$

First, we compute the model outputs of 1-local measurements. Define the 1-qubit observables in Fig. 5 using (7),

$$H_1 = \begin{pmatrix} h_{11}^{(1)} & h_{12}^{(1)} \\ \bar{h}_{12}^{(1)} & h_{22}^{(1)} \end{pmatrix}, \quad H_2 = \begin{pmatrix} h_{11}^{(2)} & h_{12}^{(2)} \\ \bar{h}_{12}^{(2)} & h_{22}^{(2)} \end{pmatrix}$$

with $h_{11}^{(i)}, h_{22}^{(i)} \in \mathbb{R}$, $h_{12}^{(i)} \in \mathbb{C}$; the corresponding 1-locals are,

$$\begin{aligned} \widetilde{H}_1 = H_1 \otimes I &= \begin{pmatrix} h_{11}^{(1)} & 0 & h_{12}^{(1)} & 0 \\ 0 & h_{11}^{(1)} & 0 & h_{12}^{(1)} \\ \bar{h}_{12}^{(1)} & 0 & h_{22}^{(1)} & 0 \\ 0 & \bar{h}_{12}^{(1)} & 0 & h_{22}^{(1)} \end{pmatrix}, \\ \widetilde{H}_2 = I \otimes H_2 &= \begin{pmatrix} h_{11}^{(2)} & h_{12}^{(2)} & & \mathbf{0} \\ \bar{h}_{12}^{(2)} & h_{22}^{(2)} & & \mathbf{0} \\ & & h_{11}^{(2)} & h_{12}^{(2)} \\ & & \bar{h}_{12}^{(2)} & h_{22}^{(2)} \end{pmatrix} \end{aligned} \quad (16)$$

For simplification, we consider the special case of real encoded state $(v_1, v_2, v_3, v_4) \in \mathbb{R}^4$. In this case, the 1-local observables have the following expectation values as model outputs:

$$\begin{aligned} \langle \widetilde{H}_1 \rangle_\psi &= h_{11}^{(1)}(v_1^2 + v_2^2) + 2\Re h_{12}^{(1)}(v_1 v_3 + v_2 v_4) + h_{22}^{(1)}(v_3^2 + v_4^2) \\ \langle \widetilde{H}_2 \rangle_\psi &= h_{11}^{(2)}(v_1^2 + v_3^2) + 2\Re h_{12}^{(2)}(v_1 v_2 + v_3 v_4) + h_{22}^{(2)}(v_2^2 + v_4^2) \end{aligned} \quad (17)$$

Next, when the 1-local measurements are incorporated with a variational rotation $R := R_y(\theta_1) \otimes R_y(\theta_2)$ of parameters (θ_1, θ_2) (Fig. 6). The resulting expectation values are given by Equation (18) and (19).

$$\begin{aligned}
\langle R^\dagger \widetilde{H}_1 R \rangle_\psi &= h_{11}^{(1)} \left((v_1^2 + v_2^2) \cos^2 \frac{\theta_1}{2} + (v_3^2 + v_4^2) \sin^2 \frac{\theta_1}{2} - (v_1 v_3 + v_2 v_4) \sin \theta_1 \right) \\
&\quad + \Re h_{12}^{(1)} \left(2 \cos \theta_1 (v_1 v_3 + v_2 v_4) + (v_1^2 + v_2^2 - v_3^2 - v_4^2) \sin \theta_1 \right) \\
&\quad + h_{22}^{(1)} \left((v_1^2 + v_2^2) \sin^2 \frac{\theta_1}{2} + (v_3^2 + v_4^2) \cos^2 \frac{\theta_1}{2} + (v_1 v_3 + v_2 v_4) \sin \theta_1 \right) \quad (18)
\end{aligned}$$

$$\begin{aligned}
\langle R^\dagger \widetilde{H}_2 R \rangle_\psi &= h_{11}^{(2)} \left((v_1^2 + v_3^2) \cos^2 \frac{\theta_2}{2} + (v_2^2 + v_4^2) \sin^2 \frac{\theta_2}{2} - (v_1 v_2 + v_3 v_4) \sin \theta_2 \right) \\
&\quad + \Re h_{12}^{(2)} \left(2 \cos \theta_2 (v_1 v_2 + v_3 v_4) + (v_1^2 - v_2^2 + v_3^2 - v_4^2) \sin \theta_2 \right) \\
&\quad + h_{22}^{(2)} \left((v_1^2 + v_3^2) \sin^2 \frac{\theta_2}{2} + (v_2^2 + v_4^2) \cos^2 \frac{\theta_2}{2} + (v_1 v_2 + v_3 v_4) \sin \theta_2 \right) \quad (19)
\end{aligned}$$

Comparing equations (17)-(19), we see the coupling between the observable elements $h_{jk}^{(i)}$ and feature vector (v_1, \dots, v_4) is more versatile in (18), (19) than in the 1-local case (17). For instance, in (18), $h_{11}^{(1)}$ perceives all four features v_1 to v_4 at once, whereas in (17) $h_{11}^{(1)}$, it only sees v_1, v_2 , not knowing the existence of v_3, v_4 . Thus, when optimizing variable $h_{jk}^{(i)}$, (18) provides more information from input, giving better guidance than the pure 1-local adaptation (17). This can also be seen by turning off the rotation $\theta_1 = \theta_2 = 0$ in (18), (19).

From the comparison, we observe that introducing rotations enhances feature mixing within the quantum state, helping to compensate for the limited connectivity in lower k -local measurements. The above argument completes the illustration of the first subset relation in (*).

As discussed in Sec. III-C, the full ANO (2-local in this case) includes all possible Hermitian matrices that can be reached by applying rotations to 1-local observables, which therefore implies the second subset relation in (*). The trade-off, however, is to increase k -locality to substitute for variational rotations. ■

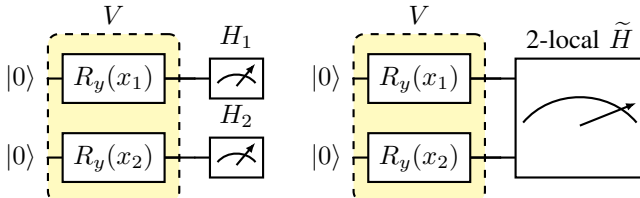


Fig. 5: 2-qubit circuits using *only*: [left] 1-local, and [right] 2-local \tilde{H} , without any entangling or variational rotations.

The above heuristic shows how variational rotations increase feature interactions within the ANO, enhancing information mixing. This suggests that combining variational rotations with smaller k -local ANO can serve as an efficient alternative to the full adaptive observable ($k = n$). To validate this insight, we conduct experiments and introduce two local measurement configurations designed to improve feature interaction

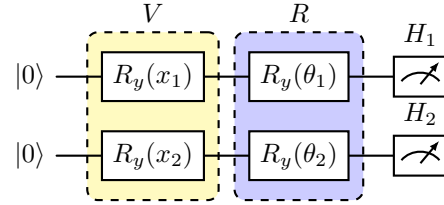


Fig. 6: 1-local ANO + variational rotation R .

efficiency. The details are presented in the following section.

IV. EXPERIMENTS

We evaluate the efficient k -local observables joining rotations in Sec. III-D with two classification tasks: the **Banknote Authentication** dataset [44] and **MNIST** [45].

A. Experimental setup

Datasets: 1) The Banknote Authentication consists of 1,372 samples, each with 4-dimensional features extracted from wavelet-transformed images of banknotes: variance, skewness, kurtosis, and entropy. The task is binary classification—determining whether a banknote is genuine or forged. The dataset is split 90/10 into training and testing sets.

2) The MNIST comprises grayscale images of handwritten digits (0–9), each of size 28×28 , for a 10-class classification task. Due to computational constraints, the images are resized to 4×4 via interpolation and use a subset of 10,000 samples. A random split of 9,000 training and 1,000 test images is performed for evaluation.

Circuit structure: The circuit structure before measurements in all experiments is shown in Fig. 1. Unless specified otherwise, the same architecture is employed throughout.

An input $x \in \mathbb{R}^n$ is encoded into an n -qubit system via (3) from an initial state $|0\rangle^{\otimes n}$. Next, the variational $U(\theta)$ in (4) is applied, consisting of (a) a chain of CNOT gates between adjacent qubits in a linear topology $(1, 2), (2, 3), \dots, (n-1, n)$ and (b) a tensor product of 1-qubit rotations R_y applied independently to each qubit with parameter θ . This layer is repeated $L = 4$ times in all experiments.

Two Measurement Schemes: The following experiments employ two distinct measurement schemes that differ in how qubits are grouped for measurement. See Fig. 7, 8 for illustrations. Qubit groupings are indicated by parentheses, e.g., $(2, 3)$ denotes a joint measurement on qubits 2 & 3.

1) **Sliding k -Local Measurements:** This scheme applies a sliding window of k -local measurement over an n -qubit system in a *cyclic* fashion, forming n overlapping k -qubit groups. Each group is measured with a distinct k -local ANO observable. For example, with $k = 2$ and $n = 3$, the measurement groups are:

$$(1, 2), (2, 3), (3, 1) \quad (\text{see Fig. 7})$$

Each group, measured by a k -local ANO, produces a scalar output, yielding n values in total. If the desired output dimension $d_{\text{out}} \leq n$, only the first d_{out} outputs are retained. This approach provides structured, locality-aware measurements with efficient reuse across inputs. This approach is similar to the classical Convolution Neural Network (CNN) using finite horizon kernels (small k -local ANOs in our case) to patch local patterns into a global representation.

Although this cyclic sliding k -local ANO captures local structure, its parameter count grows exponentially with k . To further reduce parameters while considering various feature interactions, another 2-local measurement strategy can be conceived to evaluate all qubit pairs (or a selected subset) within a defined set as follows.

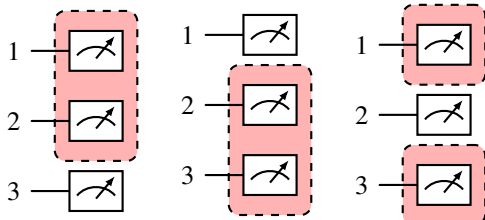


Fig. 7: [Scheme 1] Sliding k -local ANO with cyclic measurements. Here $k = 2$, $n = 3$.

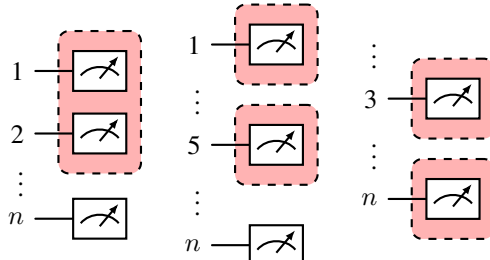


Fig. 8: [Scheme 2] Choose a subset $S \subseteq \{1, \dots, n\}$ and measure every possible pair in S with a 2-local ANO to yield a $(|S| \choose 2)$ -dimensional output.

2) **Pairwise Combinatorial Measurement:** This scheme begins by selecting an observing qubit subset S from the total n , $S \subseteq \{1, \dots, n\}$. For every distinct qubit pair (i, j) within S , a dedicated 2-local ANO measurement is performed, see Fig. 8. For example, in a 6-qubit system:

- If $S = \{1, 2, 3, 4, 5, 6\}$, then $\binom{6}{2} = 15$ pairs are measured.
- If $S = \{1, 3, 5\}$, then 3 pairs: $(1, 3)$, $(1, 5)$, $(3, 5)$ are measured.

The total number of pairwise measurements is $\binom{|S|}{2}$, which defines the output dimension of this scheme. If this exceeds the desired output size, a linear layer is applied to project the output to the target dimension.

We emphasize that although each 2-local measurement captures only localized information, the combinatorial coverage within S allows these segments to collectively uncover global data structure.

This scheme is specifically designed to overcome the parameter-efficiency concern while retaining feature interaction capability. By solely relying on 2-local (4×4 Hermitians) observables for each qubit pair, it tactically avoids the rapid parameter growth in higher k -local ANO while allowing pairwise feature mixtures.

B. Results

1) **Banknote:** Given the small feature dimension (4 features), we directly evaluate sliding k -local ANO of $k = 1, 2, 3$ in (7) and compare them to a fixed Pauli measurement baseline. For each setup, we conduct ablation studies by removing rotational gates (“w/o Rs” in Table I) to assess their impact. Each experiment is repeated over 10 independent trials, with results summarized in Table I.

First, we observe that even the simplest 1-local measurement significantly outperforms the fixed Pauli baseline. This conforms with the theoretical insights given in Sec. III-C that learnable Hermitian operators flexibly expand eigenvalues for local qubit groups. However, when removing the rotation gates, the performance drops as expected. As discussed in Example 1, this is because rotation gates enhance feature mixing and non-linear interactions so that the effects are particularly pronounced in the 1-local setting.

Interestingly, the effect of needing rotation gates diminishes as k increases. In the 3-local case, performance remains essentially unchanged with or without the rotational layer.

In other words, as the non-local k increases, the benefit of having rotations becomes less significant. For small k (e.g., 1-local), rotation gates play a critical role in improving model expressivity—by mixing features and introducing non-linearities. However, when higher k -locals are involved, adaptive observables themselves already capture more complex, non-local correlations. As a result, the additional expressivity gained from including rotational gates becomes less crucial, and removing them has a smaller impact on performance.

Overall, performance improves with increasing k , benefiting from the richer structure of higher-order measurements. Nevertheless, due to the small input dimension, the 3-local slightly shows signs of overfitting, leading to a marginal drop

in accuracy compared to the 2-local case. Thus, the best overall performance is attained by 2-local measurements with variational rotations.

Fig. 9 shows test accuracy over training epochs, highlighting the performance gap between the fixed Pauli baseline and the proposed k -local ANO. Notably, the 2-local and 3-local models converge rapidly with narrow confidence intervals, demonstrating stable learning ability.

2) **MNIST**: By resizing images to 4×4 , we evaluate the two measurement schemes mentioned in Sec. IV-A1 and Sec. IV-A2. Each setup is repeated over 5 trials. Results are summarized in Table II and plotted in Fig. 10.

Sliding k -local Measurement.

In this scheme, we observe a consistent trend of accuracy improvement as k increases, verifying the benefit of broader qubit interactions in measurement. However, the marginal gains (in test accuracy) diminish with each increment of k , Table II (a):

- 1-local \rightarrow 2-local: +9%
- 2-local \rightarrow 3-local: +8%
- 3-local \rightarrow 4-local: +6%
- 4-local \rightarrow 5-local: +4%.

Note the last observation from 4-local \rightarrow 5-local only improves 4%. This diminishing return suggests a limit to the performance gains obtainable solely through increasing k .

However, learnable parameters grow quickly with k . Moving from 2-local \rightarrow 5-local increases parameters by 46x (from $224 \rightarrow 10,304$), deriving only 17% accuracy increase. This indicates a trade-off: while k -local measurements provide high model fitting capability, they tend to become redundant or inefficient when data is simple.

Pairwise Combinatorial Measurement.

We explore this scheme with three different cases of observing subset \mathcal{S} , stated in Sec. IV-A2:

- $\mathcal{S} = \{\text{all 16 qubits}\}$,
- $\mathcal{S} = \{1, 3, 5, 7, 9, 11, 13, 15\}$ (evenly-spaced 8 qubits)
- $\mathcal{S} = \{1, 4, 7, 10, 13, 16\}$ (sparse-distributed 6 qubits).

Notably, for the experiments in this scheme with MNIST, we *completely* eliminate rotation gates to move beyond the traditional VQC framework.

Although this measurement scheme reduces the parameter numbers, performance remains competitive. Table II (a) shows that a full 16-qubit (4×4 images) ANO using pairwise measurement achieves the highest accuracy of 82% with only 3,130 parameters, outperforming the 5-local model of 79.1% accuracy using over three times as many parameters (10,304).

Similarly, the 8-qubit ANO in this scheme achieves 74.9% accuracy with just 738 parameters, comparable to the 4-local model's 75.2% but with more than 3x fewer parameters. These results demonstrate that pairwise measurement modeling, even in a limited 2-local form, can be highly effective when an observing set \mathcal{S} is suitably chosen.

TABLE I: [**k -local Test Accuracy on Banknote**] k -local ANO outperform the fixed Pauli baseline. Rotation gates (“Rs”) boost performance, especially for lower k . For higher k , the impact of Rs diminishes.

	Param #	Acc (%), w/ Rs	Param #	Acc (%), w/o Rs
Pauli	16	89.0 ± 0.4	–	–
1-local	24 (8+16)	99.3 ± 0.8	8	73.3 ± 1.0
2-local	48 (32+16)	99.7 ± 0.4	32	98.4 ± 0.3
3-local	144 (128+16)	99.5 ± 0.4	128	99.4 ± 0.4

Collectively, these experiments reveal the potential of the proposed non-local ANO to be considered as an attempt beyond conventional VQC.

TABLE II: [**k -local ANO on MNIST**] Accuracy increases with larger k but shows diminishing gains in the cases of sliding k -local ANO. Pairwise Combinatorial Measurement yields strong performance with fewer parameters and without the rotation gates, highlighting its efficiency in capturing feature interactions.

(a) Sliding k -local		
	Param #	Test accuracy (%)
1-local	104	52.3 ± 1.9
2-local	224	61.7 ± 2.2
3-local	704	69.3 ± 1.0
4-local	2624	75.2 ± 0.8
5-local	10,304	79.1 ± 0.9

(b) Pairwise Combinatorial		
	Param #	Test accuracy (%)
6 qubits	400	62.4 ± 0.6
8 qubits	738	74.9 ± 0.6
16 qubits (all)	3130	82.0 ± 1.1

V. CONCLUSION

In this work, we introduced an adaptive non-local measurement framework for QNNs that significantly enhances model expressivity by replacing traditional fixed Pauli matrices with trainable non-local Hermitian operators.

Inspired by the Heisenberg representation, we consider dynamical Hermitian observables with evolving parameters (Sec. III-B), in contrast to the static observables of standard VQCs in the Schrödinger picture (Sec. III-A). From this viewpoint, VQC and ANO appear to establish a one-to-one correspondence (Fig. 3), where every variational rotation $U(\theta)$ from VQC corresponds to a transition of an observable in the Hermitian space.

Investigating the quotient structure on Hermitian space by unitary similarity (Theorem, Sec. III-C) indicates that the conventional VQC is, in fact, only a special case of the ANO framework since the nature of a fixed observable necessarily restricts the VQC within only one equivalence class (Fig. 4). That is, the full ANO contains higher model complexity than the conventional VQC. While fully ANO makes it possible to eliminate variational rotation gates entirely, Sec. III-D shows

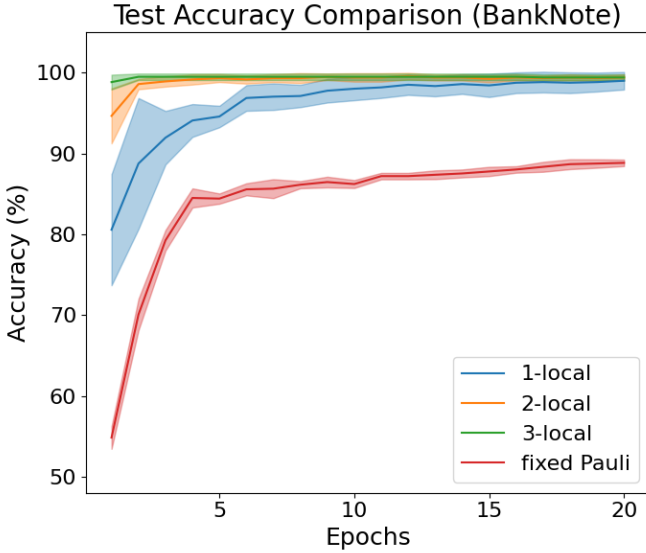


Fig. 9: **Banknote test accuracy curves over epochs.** k -local models outperform the fixed Pauli baseline, with higher k yielding faster convergence and better accuracy.

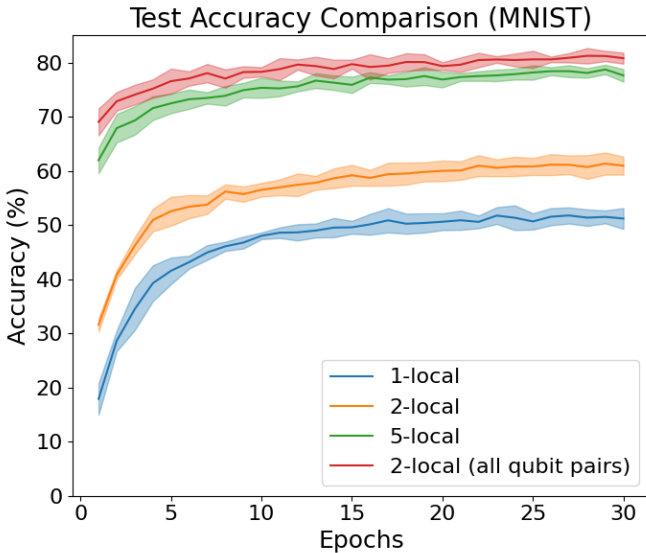


Fig. 10: **MNIST test accuracy curves over epochs.** The pairwise 2-local model over all qubits (in red) consistently outperforms the best k -local methods.

that strategically reintroducing rotations into smaller non-local observables can enhance qubit connectivity. This offers a parameter-efficient alternative that retains the expressive power of ANO.

To validate our theoretical framework, we conduct comprehensive simulations on two tasks, the Banknote Authentication and MNIST datasets. Due to the versatility of non-local ANO, we design two measurement schemes: sliding k -local measurements and pairwise combinatorial measurements. Results show that sliding significantly boosts classification

performance, especially when paired with variational rotation gates. However, as the non-local size k increases, the benefit of rotations diminishes, suggesting that the measurement observables alone can capture rich non-local correlations.

In contrast, pairwise combinatorial measurement offers a more parameter-efficient alternative. It reduces computational complexity and model size while maintaining, or even surpassing, the performance of more parameter-heavy k -local configurations.

Together, the ANO framework and these empirical studies reveal new directions for building expressive yet efficient QNNs, to provide varieties of quantum learning circuits.

REFERENCES

- [1] J. R. McClean, J. Romero, R. Babbush, and A. Aspuru-Guzik, “The theory of variational hybrid quantum-classical algorithms,” *New Journal of Physics*, vol. 18, no. 2, p. 023023, 2016.
- [2] M. Cerezo, A. Arrasmith, R. Babbush, S. C. Benjamin, S. Endo, K. Fujii, J. R. McClean, K. Mitarai, X. Yuan, L. Cincio *et al.*, “Variational quantum algorithms,” *Nature Reviews Physics*, vol. 3, no. 9, pp. 625–644, 2021.
- [3] K. Bharti, A. Cervera-Lierta, T. H. Kyaw, T. Haug, S. Alperin-Lea, A. Anand, M. Degroote, H. Heimonen, J. S. Kottmann, T. Menke *et al.*, “Noisy intermediate-scale quantum algorithms,” *Reviews of Modern Physics*, vol. 94, no. 1, p. 015004, 2022.
- [4] X. Bonet-Monroig, H. Wang, D. Vermetten, B. Senjean, C. Moussa, T. Bäck, V. Dunjko, and T. E. O’Brien, “Performance comparison of optimization methods on variational quantum algorithms,” *Physical Review A*, vol. 107, no. 3, p. 032407, 2023.
- [5] K. Mitarai, M. Negoro, M. Kitagawa, and K. Fujii, “Quantum circuit learning,” *Physical Review A*, vol. 98, no. 3, p. 032309, 2018.
- [6] M. Cerezo, A. Sone, T. Volkoff, L. Cincio, and P. J. Coles, “Cost function dependent barren plateaus in shallow parametrized quantum circuits,” *Nature communications*, vol. 12, no. 1, p. 1791, 2021.
- [7] M. Ostaszewski, E. Grant, and M. Benedetti, “Structure optimization for parameterized quantum circuits,” *Quantum*, vol. 5, p. 391, 2021.
- [8] C. Cade, L. Mineh, A. Montanaro, and S. Stanisic, “Strategies for solving the fermi-hubbard model on near-term quantum computers,” *Physical Review B*, vol. 102, no. 23, p. 235122, 2020.
- [9] S. Y.-C. Chen, C.-M. Huang, C.-W. Hsing, H.-S. Goan, and Y.-J. Kao, “Variational quantum reinforcement learning via evolutionary optimization,” *Machine Learning: Science and Technology*, vol. 3, no. 1, p. 015025, 2022.
- [10] A. Peruzzo, J. McClean, P. Shadbolt, M.-H. Yung, X.-Q. Zhou, P. J. Love, A. Aspuru-Guzik, and J. L. O’Brien, “A variational eigenvalue solver on a photonic quantum processor,” *Nature communications*, vol. 5, no. 1, p. 4213, 2014.
- [11] A. Kandala, A. Mezzacapo, K. Temme, M. Takita, M. Brink, J. M. Chow, and J. M. Gambetta, “Hardware-efficient variational quantum eigensolver for small molecules and quantum magnets,” *nature*, vol. 549, no. 7671, pp. 242–246, 2017.
- [12] H. R. Grimsley, S. E. Economou, E. Barnes, and N. J. Mayhall, “An adaptive variational algorithm for exact molecular simulations on a quantum computer,” *Nature communications*, vol. 10, no. 1, p. 3007, 2019.
- [13] E. Farhi and H. Neven, “Classification with quantum neural networks on near term processors,” *arXiv preprint arXiv:1802.06002*, 2018.
- [14] S. Y.-C. Chen, C.-M. Huang, C.-W. Hsing, and Y.-J. Kao, “An end-to-end trainable hybrid classical-quantum classifier,” *Machine Learning: Science and Technology*, vol. 2, no. 4, p. 045021, 2021.
- [15] J. Qi, C.-H. H. Yang, and P.-Y. Chen, “Qtn-vqc: An end-to-end learning framework for quantum neural networks,” *Physica Scripta*, vol. 99, 12 2023.
- [16] S. Y.-C. Chen, T.-C. Wei, C. Zhang, H. Yu, and S. Yoo, “Quantum convolutional neural networks for high energy physics data analysis,” *Physical Review Research*, vol. 4, no. 1, p. 013231, 2022.
- [17] M. Chehimi, S. Y.-C. Chen, W. Saad, and S. Yoo, “Federated quantum long short-term memory (fedqlstm),” *Quantum Machine Intelligence*, vol. 6, no. 2, p. 43, 2024.

- [18] S. Y.-C. Chen, “Learning to program variational quantum circuits with fast weights,” *arXiv preprint arXiv:2402.17760*, 2024.
- [19] J. Romero, J. P. Olson, and A. Aspuru-Guzik, “Quantum autoencoders for efficient compression of quantum data,” *Quantum Science and Technology*, vol. 2, no. 4, p. 045001, 2017.
- [20] S. Y.-C. Chen, C.-H. H. Yang, J. Qi, P.-Y. Chen, X. Ma, and H.-S. Goan, “Variational quantum circuits for deep reinforcement learning,” *IEEE access*, vol. 8, pp. 141 007–141 024, 2020.
- [21] C. Zoufal, A. Lucchi, and S. Woerner, “Quantum generative adversarial networks for learning and loading random distributions,” *npj Quantum Information*, vol. 5, no. 1, p. 103, 2019.
- [22] S. S. Li, X. Zhang, S. Zhou, H. Shu, R. Liang, H. Liu, and L. P. Garcia, “Pqlm-multilingual decentralized portable quantum language model,” in *ICASSP 2023-2023 IEEE International Conference on Acoustics, Speech and Signal Processing (ICASSP)*. IEEE, 2023, pp. 1–5.
- [23] C.-H. H. Yang, J. Qi, S. Y.-C. Chen, Y. Tsao, and P.-Y. Chen, “When bert meets quantum temporal convolution learning for text classification in heterogeneous computing,” in *ICASSP 2022-2022 IEEE International Conference on Acoustics, Speech and Signal Processing (ICASSP)*. IEEE, 2022, pp. 8602–8606.
- [24] R. Di Sipio, J.-H. Huang, S. Y.-C. Chen, S. Mangini, and M. Worring, “The dawn of quantum natural language processing,” in *ICASSP 2022-2022 IEEE International Conference on Acoustics, Speech and Signal Processing (ICASSP)*. IEEE, 2022, pp. 8612–8616.
- [25] J. Stein, I. Christ, N. Kraus, M. B. Mansky, R. Müller, and C. Linnhoff-Popien, “Applying qnlp to sentiment analysis in finance,” in *2023 IEEE International Conference on Quantum Computing and Engineering (QCE)*, vol. 2. IEEE, 2023, pp. 20–25.
- [26] H.-Y. Lin, H.-H. Tseng, S. Y.-C. Chen, and S. Yoo, “Quantum gradient class activation map for model interpretability,” in *2024 IEEE Workshop on Signal Processing Systems (SiPS)*. IEEE, 2024, pp. 165–170.
- [27] M. Benedetti, E. Lloyd, S. Sack, and M. Fiorentini, “Parameterized quantum circuits as machine learning models,” *Quantum science and technology*, vol. 4, no. 4, p. 043001, 2019.
- [28] D. Ristè, M. P. Da Silva, C. A. Ryan, A. W. Cross, A. D. Córcoles, J. A. Smolin, J. M. Gambetta, J. M. Chow, and B. R. Johnson, “Demonstration of quantum advantage in machine learning,” *npj Quantum Information*, vol. 3, no. 1, p. 16, 2017.
- [29] S. Jerbi, L. J. Fiderer, H. Poulsen Nautrup, J. M. Kübler, H. J. Briegel, and V. Dunjko, “Quantum machine learning beyond kernel methods,” *Nature Communications*, vol. 14, no. 1, p. 517, 2023.
- [30] I. Cong, S. Choi, and M. D. Lukin, “Quantum convolutional neural networks,” *Nature Physics*, vol. 15, no. 12, pp. 1273–1278, 2019.
- [31] S. Y.-C. Chen, H.-H. Tseng, H.-Y. Lin, and S. Yoo, “Learning to measure quantum neural networks,” *arXiv preprint arXiv:2501.05663*, 2025.
- [32] A. Elben, B. Vermersch, C. F. Roos, and P. Zoller, “Statistical correlations between locally randomized measurements: A toolbox for probing entanglement in many-body quantum states,” *Physical Review A*, vol. 99, no. 5, p. 052323, 2019.
- [33] A. Elben, B. Vermersch, R. Van Bijnen, C. Kokail, T. Brydges, C. Maier, M. K. Joshi, R. Blatt, C. F. Roos, and P. Zoller, “Cross-platform verification of intermediate scale quantum devices,” *Physical review letters*, vol. 124, no. 1, p. 010504, 2020.
- [34] D. Zhu, Z.-P. Cian, C. Noel, A. Risinger, D. Biswas, L. Egan, Y. Zhu, A. M. Green, C. H. Alderete, N. H. Nguyen *et al.*, “Cross-platform comparison of arbitrary quantum computations,” *arXiv preprint arXiv:2107.11387*, 2021.
- [35] T. Haug, C. N. Self, and M. S. Kim, “Quantum machine learning of large datasets using randomized measurements,” *Machine Learning: Science and Technology*, vol. 4, no. 1, p. 015005, 2023.
- [36] J. Malmi, K. Korhonen, D. Cavalcanti, and G. García-Pérez, “Enhanced observable estimation through classical optimization of informationally overcomplete measurement data: Beyond classical shadows,” *Physical Review A*, vol. 109, no. 6, p. 062412, 2024.
- [37] G. García-Pérez, M. A. Rossi, B. Sokolov, F. Tacchino, P. K. Barkoutsos, G. Mazzola, I. Tavernelli, and S. Maniscalco, “Learning to measure: Adaptive informationally complete generalized measurements for quantum algorithms,” *Prx quantum*, vol. 2, no. 4, p. 040342, 2021.
- [38] V. Gebhart, R. Santagati, A. A. Gentile, E. M. Gauger, D. Craig, N. Ares, L. Banchi, F. Marquardt, L. Pezze, and C. Bonato, “Learning quantum systems,” *Nature Reviews Physics*, vol. 5, no. 3, pp. 141–156, 2023.
- [39] C. C. Tannoudji, B. Diu, and F. Laloë, *Quantum mechanics*. John Wiley & Sons, 2020.
- [40] A. Y. Kitaev, A. Shen, and M. N. Vyalyi, *Classical and quantum computation*. American Mathematical Soc., 2002, no. 47.
- [41] R. Oliveira and B. M. Terhal, “The complexity of quantum spin systems on a two-dimensional square lattice,” *arXiv preprint quant-ph/0504050*, 2005.
- [42] R. A. Horn and C. R. Johnson, *Matrix analysis*. Cambridge university press, 2012.
- [43] Z. Allen-Zhu, Y. Li, and Z. Song, “A convergence theory for deep learning via over-parameterization,” in *International conference on machine learning*. PMLR, 2019, pp. 242–252.
- [44] V. Lohweg, “Banknote Authentication,” UCI Machine Learning Repository, 2012, DOI: <https://doi.org/10.24432/C55P57>.
- [45] Y. LeCun, L. Bottou, Y. Bengio, and P. Haffner, “Gradient-based learning applied to document recognition,” *Proceedings of the IEEE*, vol. 86, no. 11, pp. 2278–2324, 1998.